

A conservative numerical method for the fractional nonlinear Schrödinger equation in two dimensions

Rongpei Zhang^{1,*}, Yong-Tao Zhang², Zhen Wang³, Bo Chen⁴ & Yi Zhang¹

¹*School of Mathematics and Systematic Sciences, Shenyang Normal University, Shenyang 110034, China;*

²*Department of Applied and Computational Mathematics and Statistics, University of Notre Dame, Notre Dame, IN 46556, USA;*

³*College of Mathematics and Systems Science, Shandong University of Science and Technology, Qingdao 266590, China;*

⁴*College of Mathematics and Statistics, Shenzhen University, Shenzhen 518060, China*

Email: rzhang1@nd.edu, yizhang10@nd.edu, wangzhen@sdust.edu.cn, chenbo@szu.edu.cn, yizhang729@gmail.com

Received February 2, 2018; accepted September 3, 2018; published online May 16, 2019

Abstract This paper proposes and analyzes an efficient finite difference scheme for the two-dimensional nonlinear Schrödinger (NLS) equation involving fractional Laplacian. The scheme is based on a weighted and shifted Grünwald-Letnikov difference (WSGD) operator for the spatial fractional Laplacian. We prove that the proposed method preserves the mass and energy conservation laws in semi-discrete formulations. By introducing the differentiation matrices, the semi-discrete fractional nonlinear Schrödinger (FNLS) equation can be rewritten as a system of nonlinear ordinary differential equations (ODEs) in matrix formulations. Two kinds of time discretization methods are proposed for the semi-discrete formulation. One is based on the Crank-Nicolson (CN) method which can be proved to preserve the fully discrete mass and energy conservation. The other one is the compact implicit integration factor (cIIF) method which demands much less computational effort. It can be shown that the cIIF scheme can approximate CN scheme with the error $O(\tau^2)$. Finally numerical results are presented to demonstrate the method's conservation, accuracy, efficiency and the capability of capturing blow-up.

Keywords fractional nonlinear Schrödinger equation, weighted and shifted Grünwald-Letnikov difference, compact integration factor method, conservation

MSC(2010) 65N06, 35R11

Citation: Zhang R P, Zhang Y-T, Wang Z, et al. A conservative numerical method for the fractional nonlinear Schrödinger equation in two dimensions. *Sci China Math*, 2019, 62: 1997–2014, <https://doi.org/10.1007/s11425-018-9388-9>

1 Introduction

The fractional nonlinear Schrödinger equations (FNLS) are generalizations of the classical (non-fractional) nonlinear Schrödinger equation which plays an important role in many fields of physics. Laskin [17, 18] derived the FNLS with quantum Riesz space-fractional derivative by extending the Feynman path integral to a Lévy one. The FNLS equations can also be found in the continuum limit of discrete models with long range interaction [15], in the mathematical description of Boson-stars [9, 19], and in some models of water wave dynamics [12, 28].

* Corresponding author

In this paper, we consider the following two-dimensional symmetric space-fractional FNLS equation on a bounded domain $[a, b] \times [c, d]$:

$$i \frac{\partial u}{\partial t} = \frac{\partial^\alpha u}{\partial |x|^\alpha} + \frac{\partial^\alpha u}{\partial |y|^\alpha} + \beta |u|^2 u, \tag{1.1}$$

where $i = \sqrt{-1}$ is the complex unit, $u = u(x, y, t)$ is a complex-valued function, $1 < \alpha \leq 2$. The Riesz fractional derivatives $\frac{\partial^\alpha u}{\partial |x|^\alpha}$ and $\frac{\partial^\alpha u}{\partial |y|^\alpha}$ are defined as follows:

$$\frac{\partial^\alpha u}{\partial |x|^\alpha} = \begin{cases} \frac{-1}{2 \cos \frac{\pi\alpha}{2}} ({}_a D_x^\alpha u + {}_x D_b^\alpha u), & 1 < \alpha < 2, \\ \frac{\partial^2 u}{\partial x^2}, & \alpha = 2, \end{cases} \tag{1.2}$$

$$\frac{\partial^\alpha u}{\partial |y|^\alpha} = \begin{cases} \frac{-1}{2 \cos \frac{\pi\alpha}{2}} ({}_c D_y^\alpha u + {}_y D_d^\alpha u), & 1 < \alpha < 2, \\ \frac{\partial^2 u}{\partial y^2}, & \alpha = 2. \end{cases} \tag{1.3}$$

The left and right Riemann-Liouville fractional derivatives, ${}_a D_x^\alpha$ and ${}_x D_b^\alpha$, are respectively defined as

$${}_a D_x^\alpha u = \frac{1}{\Gamma(2-\alpha)} \frac{\partial^2}{\partial x^2} \int_a^x \frac{u(\xi, y)}{(\xi-x)^{(\alpha-1)}} d\xi, \quad {}_x D_b^\alpha u = \frac{1}{\Gamma(2-\alpha)} \frac{\partial^2}{\partial x^2} \int_x^b \frac{u(\xi, y)}{(x-\xi)^{(\alpha-1)}} d\xi, \tag{1.4}$$

where $\Gamma(\cdot)$ denotes the standard Gamma function. It is noted that, when $\alpha = 2$, this equation reduces to the classical cubic nonlinear Schrödinger (NLS) equation.

Remark 1.1. In this paper, the fractional Laplacian operator is represented by a sequential Riesz fractional-order derivative. There are also other definitions for the fractional Laplacian operator. For example the fractional Laplacian can also be defined through the Fourier transform [17]. We choose Riesz fractional-order derivative because the fractional Laplacian operator with the Fourier transform breaches the principle of locality in physics and cannot accommodate boundary conditions on finite domains [36]. As pointed in [22], the Lévy flight is equivalent to the Riesz fractional order space operator. Thus the fractional order operators of fractional calculus have a direct representation in the extended stochastic models of the conventional random walk. The sequential Riesz fractional-order Laplacian operator follows from the introduction of an inverse power law distribution of jump lengths. We also note that the fractional Laplacians defined by Riesz fractional derivative and Fourier transform formulations are not equivalent, except for certain special cases. For example, in one dimension with zero Dirichlet boundary conditions, these two formulations are the same [35]. However, in two dimensions, the two formulations are different [7]. In this paper, we use $(-\Delta^*)^{\alpha/2}$ to represent the sequential fractional Laplacian operator, i.e., that $(-\Delta^*) = \frac{\partial^\alpha u}{\partial |x|^\alpha} + \frac{\partial^\alpha u}{\partial |y|^\alpha}$. The difference between the operator $(-\Delta^*)^{\alpha/2}$ and the fractional Laplacian operator $(-\Delta)^{\alpha/2}$ lies in their Fourier transforms. The Fourier transform of $(-\Delta)^{\alpha/2}$ is

$$\mathcal{F}((-\Delta)^{\alpha/2} v) = (|\omega_1|^2 + |\omega_2|^2)^{\alpha/2} \hat{v}(\omega_1 + \omega_2),$$

where $\hat{v}(\omega_1 + \omega_2)$ denotes the Fourier transform of v . While the Fourier transform of $(-\Delta^*)^{\alpha/2}$ is defined as

$$\mathcal{F}((-\Delta^*)^{\alpha/2} v) = (|\omega_1|^\alpha + |\omega_2|^\alpha) \hat{v}(\omega_1 + \omega_2).$$

Similar to the cubic NLS equation case, the FNLS equation admits the following mass and energy conservation by the time evolution [33]:

$$\text{Mass : } M(t) = \|u\|_{L^2}^2 = M(0) \tag{1.5}$$

and

$$\text{Energy : } E(t) = \left\| \frac{\partial^{\frac{\alpha}{2}} u}{\partial |x|^{\frac{\alpha}{2}}} \right\|_{L^2}^2 + \left\| \frac{\partial^{\frac{\alpha}{2}} u}{\partial |y|^{\frac{\alpha}{2}}} \right\|_{L^2}^2 - \frac{\beta}{2} \|u\|_{L^4}^4 = E(0), \tag{1.6}$$

where $\|u\|_{L^2}^2$ and $\|u\|_{L^4}^4$ denote the L^2 - and L^4 -norm of $u(x, y, t)$, respectively.

For classical Schrödinger equations (where $\alpha = 2$), it is well known that the solutions of the NLS equation become singular with suitable initial condition data. Merle and Tsutsumi [24] proved that, for a blow-up solution with radially symmetric initial data, the origin is a blow-up point and an L^2 -concentration phenomenon occurs at the origin. For the FNLS equation (1.1), Boulenger et al. [3, Theorem 2] have also theoretically proved that the solution u blows up in finite time if the initial energy $E(0) < 0$. In this paper, the FNLS equation will be approximated to have a better understanding of the blow-up solutions' behavior.

As it is difficult to get the analytic solutions of FNLS equations, different types of numerical approaches to FNLS equations are proposed in recent years. Wang and Huang [32] studied an energy conservative Crank-Nicolson difference scheme for nonlinear Riesz space-fractional Schrödinger equations. Then they combined the split-step method with the alternating direction implicit (ADI) method for resolving the multi-dimensions cases [33]. Yang [37] derived a class of linearized energy-conserved finite difference schemes for nonlinear FNLS equations and the energy conservation and convergence were examined. Khaliq et al. [14] combined the fourth-order implicit-explicit time-discretization scheme with a fourth-order compact scheme in space for one-dimensional FNLS, and then extended to multi-dimensional cases by using local extrapolation of the exponential operator splitting scheme [21]. Zhao et al. [40] utilized a compact alternating direction implicit approach based on the linearized difference scheme to solve two-dimensional space-fractional FNLS equation. A Fourier spectral method for one-dimensional FNLS equation was developed by Klein et al. [16], in which the possibility of finite time blow-up and global existence were studied. Bhrawy and Abdelkawy [2] developed a shifted Legendre collocation method to numerically solve one- and two-dimensional time FNLS equations. Later, Duo and Zhang [8] proposed three Fourier spectral methods to solve the FNLS equation, and proved the mass conservation and time reversibility. Li et al. [20] proposed a Galerkin finite element method in space and the Crank-Nicolson method in time for one-dimensional FNLS equations and derived conservation analysis and convergence properties. Aboelenen [1] proposed a nodal discontinuous Galerkin method for solving the FNLS equations and proved the L^2 stability and optimal order of convergence.

For classical cubic NLS equations, a wealth of experience reveals that the conserve numerical methods are favorable because they are able to maintain the phase and shape of the waves accurately for long time integration. Extensive conservative schemes have been studied in the literature for integer order NLS equations. These methods include the spectral (pseudospectral) method [10, 39], finite difference method (FDM) [5, 6] and discontinuous Galerkin (DG) method [34, 38]. Naturally, it is also of interest to construct the conservative numerical schemes for solving the FNLS equations. The main goal of this paper is to construct a conservative and efficient difference scheme for solving the nonlinear two-dimensional FNLS equation. Considerable schemes have been devoted to approximate the Riesz fractional derivative. Meerschaert and Tadjeran [23] proposed the first-order shifted Grünwald formula. Based on the former work, Tian et al. [30] developed two types of second-order weighted and shifted Grünwald-Letnikov difference (WSGD) formulas. Recently Hou et al. [11] applied this method for solving the Allen-Cahn equation. Ortigueira [29] firstly proposed the so-called fractional central difference scheme. Then Çelik and Duman [4] analyzed this approximation and applied it to fractional diffusion equations. In this paper, we use the second-order accurate WSGD method in the space discretization. The reason for this choice is that the differential matrix of fractional derivatives is a real-value symmetric positive definite matrix and has Cholesky decomposition. This Cholesky decomposition is extremely useful for the proof of the discrete conservation laws. By using some useful lemmas, we will give the proof of the conservative properties, i.e., mass conservation and energy conservation in the semi-discrete sense.

All numerical methods for multi-dimensional nonlinear diffusion problems face the same challenge in implicit time stepping, i.e., how to efficiently solve a large nonlinear system at each time step. For the multi-dimensional FNLS equation, the most frequently used method is alternating direction implicit (ADI) [33, 40] schemes which reduce a multi-dimensional system to sets of independent one-dimensional (1D) systems. This is particularly attractive to integer order Laplacian operator, because the resulting 1D systems are tridiagonal and can be efficiently solved by using the Thomas algorithm. However, the

nonlocal property of fractional Laplacian leads to a full differential matrix and cannot apply the fast tridiagonal matrix algorithm. Moreover, the ADI methods are limited to second-order accuracy in time.

In this paper, we will apply the compact implicit integration factor (cIIF) method for the nonlinear ODEs in matrix formulation [26, 31]. After the space discretization by the WSGD method, the two-dimensional FNLS equation is now discretized into a system of nonlinear ordinary differential equations (ODEs). In order to reduce the required storage and CPU time, we introduce a compact representation for the matrix approximating the differential operator. In particular, for a two-dimensional system of $N \times N$ grid points, we can define an $N \times N$ matrix to store the unknown values at the grid points. The fractional derivative operators in the x -direction and y -direction generate two differential matrices D_x and D_y which are much smaller than the non-compact method. In the two-dimensional case the operation count of cIIF schemes is $O(N^3)$ vs. $O(N^4)$ for non-compact ones. Then the cIIF method applies matrix exponential operations sequentially in the x - and y -direction. As a result, the exponential matrices e^{D_x} and e^{D_y} can be calculated and stored in the preprocessing stage. Another novel property of the method is that the exact evaluation of the diffusion terms is decoupled from the implicit treatment of the nonlinear terms [27]. We only solve a local nonlinear system with each spatial grid point at each time-cycle. As a result, the cIIF is significantly more efficient in both storage and CPU cost for fractional diffusion problems.

The rest of the paper is organized as follows: In Section 2 we present some notations and discretize the two-dimensional FNLS equation into nonlinear ODEs in matrix formulation. Then we prove the mass and energy conservation laws in semi-discrete formulation. In Section 3, we present two kinds of time discretization methods: Crank-Nicolson (CN) and cIIF schemes. The efficiency of two methods is compared in the numerical experiments in Section 4. We compute various FNLS equations to demonstrate the convergence rates, the mass and energy conservation, and the excellent capability of capturing blow-up of the proposed scheme. Finally, we summarize our conclusion in Section 5.

2 Numerical methods

2.1 Fractional centered difference

Now we present the method for the initial value problem (1.1) with the homogeneous Dirichlet boundary condition. The spatial domain is discretized by rectangular mesh

$$T_h = \{(x_j, y_k) = (a + jh_x, c + kh_y), j = 0, 1, \dots, N_x, k = 0, 1, \dots, N_y\},$$

where $h_x = \frac{b-a}{N_x}$, $h_y = \frac{d-c}{N_y}$ with N_x and N_y two positive even integers.

Assume $U, V \in \mathbb{C}^{N_x \times N_y}$. The element-by-element multiplication and inner product between two matrices are defined as follows:

$$(U \odot V)_{j,k} = (u_{j,k} v_{j,k}) \quad (2.1)$$

and

$$(U, V) = h_x h_y \sum_{j=1}^{N_x} \sum_{k=1}^{N_y} U_{j,k} \bar{V}_{j,k}. \quad (2.2)$$

We also define the complex magnitude and norms over space $\mathbb{C}^{N_x \times N_y}$ as

$$(|U|)_{j,k} = |u_{j,k}| \quad (2.3)$$

and

$$\|U\|_p^p = h_x h_y \sum_{j=1}^{N_x} \sum_{k=1}^{N_y} |U_{j,k}|^p, \quad 0 < p < \infty, \quad (2.4)$$

where $\bar{V}_{j,k}$ denotes the conjugate of $V_{j,k}$.

In this paper, we use the second-order and third-order WSGD method [30] to approximate the Riemann-Liouville space fractional derivatives, respectively. The essential idea of this approximation is using the

weighted average to vanish the low order leading terms in asymptotic expansions for the truncation errors. The WSGD formulas for the left and right Riemann-Liouville fractional derivatives in the x -direction are defined as

$$\begin{aligned} {}_aD_x^\alpha u(x_j, y_k) &= \frac{1}{h^\alpha} \sum_{l=0}^{j+1} \omega_k^{(\alpha)} u(x_{j-l+1}, y_k) + o(h^p), \\ {}_xD_b^\alpha u(x_j, y_k) &= \frac{1}{h^\alpha} \sum_{l=0}^{N-j+1} \omega_k^{(\alpha)} u(x_{j+l-1}, y_k) + o(h^p) \end{aligned} \tag{2.5}$$

for $j = 1, \dots, N_x - 1, k = 1, \dots, N_y - 1$.

If the solution u satisfies $u \in C^4(R^2)$, the WSGD difference operator (2.5) has second-order accuracy, i.e., that $p = 2$ in (2.5) (see [13]). The coefficients $\omega_k^{(\alpha)}$ in (2.5) are given as

$$\omega_0^{(\alpha)} = \frac{\alpha}{2} g_0^{(\alpha)}, \quad \omega_k^{(\alpha)} = \frac{\alpha}{2} g_k^{(\alpha)} + \frac{2-\alpha}{2} g_{k-1}^{(\alpha)}, \quad k = 1, 2, \dots \tag{2.6}$$

with

$$g_0^{(\alpha)} = 1, \quad g_k^{(\alpha)} = \left(1 - \frac{1+\alpha}{k}\right) g_{k-1}^{(\alpha)}, \quad k = 1, 2, \dots \tag{2.7}$$

If the solution u satisfies $u \in C^5(R^2)$, the WSGD difference operator (2.5) has third-order accuracy, i.e., that $p = 3$ in (2.5) (see [13]). The coefficients in (2.5) are defined as

$$\omega_0^{(\alpha)} = \lambda_1 g_0^{(\alpha)}, \quad \omega_1^{(\alpha)} = \lambda_1 g_1^{(\alpha)} + \lambda_2 g_0^{(\alpha)}, \quad \omega_k^{(\alpha)} = \lambda_1 g_k^{(\alpha)} + \lambda_2 g_{k-1}^{(\alpha)} + \lambda_3 g_{k-2}^{(\alpha)}, \quad k \geq 2, \tag{2.8}$$

where $\lambda_1 = \frac{5\alpha}{24} + \frac{\alpha^2}{8}, \lambda_2 = 1 + \frac{\alpha}{12} - \frac{\alpha^2}{4}, \lambda_3 = -\frac{7\alpha}{24} + \frac{\alpha^2}{8}$. The left and right Riemann-Liouville fractional derivatives in the y -direction, ${}_cD_y^\alpha$ and ${}_yD_d^\alpha$, can be discretized in the similar way.

Based on the discretization of Riemann-Liouville fractional derivatives, the Riesz fractional derivatives in the x -direction can be discretized as

$$\begin{aligned} \frac{\partial^\alpha u(x_j, y_k)}{\partial |x|^\alpha} &= \frac{-1}{2 \cos \frac{\pi\alpha}{2}} ({}_aD_x^\alpha u(x_j, y_k) + {}_xD_b^\alpha u(x_j, y_k)) \\ &= \frac{-1}{2 \cos \frac{\pi\alpha}{2}} \left(\frac{1}{h^\alpha} \sum_{l=0}^{j+1} \omega_k^{(\alpha)} u(x_{j-l+1}, y_k) + \frac{1}{h^\alpha} \sum_{l=0}^{N-j+1} \omega_k^{(\alpha)} u(x_{j+l-1}, y_k) \right) + o(h^p), \end{aligned} \tag{2.9}$$

with $p = 2$ for second-order and $p = 3$ for third-order approximation. Riesz fractional derivatives in the y -direction can be discretized in the similar way and we omit it.

We adopt a matrix representation for u , defining $U = (u_{j,k}) \in \mathbb{C}^{N_x-1 \times N_y-1}$ as the matrix formed by the numerical solutions of u at the nodes (x_j, y_k) :

$$U = \begin{pmatrix} u_{1,1} & u_{1,2} & \cdots & u_{1,N_y-1} \\ u_{2,1} & u_{2,2} & \cdots & u_{2,N_y-1} \\ \vdots & \vdots & \ddots & \vdots \\ u_{N_x-1,1} & u_{N_x-1,2} & \cdots & u_{N_x-1,N_y-1} \end{pmatrix}. \tag{2.10}$$

Introducing the $N \times N$ differentiation matrix of the differential operator

$$D_N = \begin{pmatrix} 2\omega_1^{(\alpha)} & \omega_0^{(\alpha)} + \omega_2^{(\alpha)} & \cdots & \omega_{N-1}^{(\alpha)} & \omega_N^{(\alpha)} \\ \omega_0^{(\alpha)} + \omega_2^{(\alpha)} & 2\omega_1^{(\alpha)} & \omega_0^{(\alpha)} + \omega_2^{(\alpha)} & \cdots & \omega_{N-1}^{(\alpha)} \\ \vdots & \omega_0^{(\alpha)} + \omega_2^{(\alpha)} & 2\omega_1^{(\alpha)} & \omega_0^{(\alpha)} + \omega_2^{(\alpha)} & \vdots \\ \omega_{N-1}^{(\alpha)} & \vdots & \ddots & \vdots & \omega_0^{(\alpha)} + \omega_2^{(\alpha)} \\ \omega_N^{(\alpha)} & \omega_{N-1}^{(\alpha)} & \cdots & \omega_0^{(\alpha)} + \omega_2^{(\alpha)} & 2\omega_1^{(\alpha)} \end{pmatrix}, \tag{2.11}$$

the difference scheme (2.9) can be written in the following matrix formulations with mesh size h :

$$\frac{\partial^\alpha u(x_j, y_k)}{\partial |x|^\alpha} = (D_x U)_{j,k} + o(h^p), \quad p = 2, 3, \tag{2.12}$$

where

$$D_x = \frac{1}{-2h_x^\alpha \cos \frac{\pi\alpha}{2}} D_{N_x-1}. \tag{2.13}$$

We adopt the similar method to discretize the Riesz fractional derivatives in the y -direction

$$\frac{\partial^\alpha u(x_j, y_k)}{\partial |y|^\alpha} = (U D_y^T)_{j,k} + o(h^2), \tag{2.14}$$

where

$$D_y = \frac{1}{-2h_y^\alpha \cos \frac{\pi\alpha}{2}} D_{N_y-1}, \tag{2.15}$$

and T denotes the transpose.

After this semi-discretization (2.12) and (2.14) in space, we get the difference scheme for the FNLS equation as follows:

$$i \frac{\partial U}{\partial t} + D_x U + U D_y^T + \beta(|U| \odot |U|) \odot U = 0. \tag{2.16}$$

2.2 Conservation

The discrete mass and energy conservation laws are generally taken into consideration in the design of the numerical schemes for the FNLS equation. The schemes preserving the mass and energy conservation appear to approximate the solution better in the long time behavior. Next, we will prove that the semi-discrete WSGD method (2.16) preserves the conservation law of the mass and energy. Before presentation of the conservation of the scheme, we give some lemmas.

Lemma 2.1 (See [30]). *The discretization matrices D_x and D_y defined in (2.13) and (2.15) are symmetric and negative definite for the second-order approximation case when $1 < \alpha \leq 2$, and for the third-order approximation case when $\frac{1+\sqrt{73}}{6} < \alpha \leq 2$.*

Lemma 2.2. *There exist real symmetric positive definite matrices L_x and L_y such that the following inner product equalities hold:*

$$(D_x U, V) = -(L_x U, L_x V), \quad (U D_y^T, V) = -(U L_y^T, V L_y^T). \tag{2.17}$$

Proof. Based on the lemma above, the matrix D_x is a real symmetric negative definite matrix. There is a real orthogonal matrix P and a real diagonal matrix $\Lambda = \text{diag}(\lambda)$ such that

$$D_x = -P \Lambda P^T = -(P \Lambda^{\frac{1}{2}} P^T)^T (P \Lambda^{\frac{1}{2}} P^T) = -L_x^T L_x, \tag{2.18}$$

where $\Lambda^{\frac{1}{2}} = \text{diag}(\lambda^{\frac{1}{2}})$. Similarly, $D_y = -L_y^T L_y$. It is easily derived that matrices L_x and L_y are real symmetric positive definite matrices.

With the decomposition (2.18), we can get

$$\begin{aligned} (D_x U, V) &= -h_x h_y \sum_{j=1}^{N_x} \sum_{k=1}^{N_y} \left[\sum_{l=1}^{N_x} \left(\sum_{m=1}^{N_x} L_{x,mj} L_{x,ml} \right) U_{lk} \right] \bar{V}_{jk} \\ &= -h_x h_y \sum_{j=1}^{N_x} \sum_{k=1}^{N_y} \left[\sum_{m=1}^{N_x} \left(\sum_{l=1}^{N_x} L_{x,ml} U_{lk} \right) L_{x,mj} \right] \bar{V}_{jk} \\ &= -h_x h_y \sum_{m=1}^{N_x} \sum_{k=1}^{N_y} \left[\left(\sum_{j=1}^{N_x} L_{x,mj} \bar{V}_{jk} \right) \left(\sum_{l=1}^{N_x} L_{x,ml} U_{lk} \right) \right] \\ &= -(L_x U, L_x V). \end{aligned}$$

The second equality $(U D_y^T, V) = -(U L_y^T, V L_y^T)$ can be proved in the same way. □

On the basis of the definition of norms (2.4), the space discrete formulations of mass and energy are defined as

$$Q_h(t) = \|U\|_2^2 \tag{2.19}$$

and

$$E_h(t) = \|L_x U\|_2^2 + \|U L_y^T\|_2^2 - \frac{\beta}{2} \|U\|_4^4 \tag{2.20}$$

corresponding to (1.5) and (1.6), respectively.

Theorem 2.3. *With the homogeneous Dirichlet boundary condition, the scheme preserves the mass conservation law:*

$$\frac{d}{dt} Q_h(t) \equiv 0. \tag{2.21}$$

Proof. By taking the inner product of (2.16) with U , we can obtain

$$i \left(\frac{dU}{dt}, U \right) + (D_x U, U) + (U D_y^T, U) + \beta ((|U| \odot |U|) \odot U, U) = 0. \tag{2.22}$$

According to Lemma 2.2, the second term becomes $(D_x U, U) = -(L_x U, L_x U) = -\|L_x U\|_2^2$. Similarly, the third term $(U D_y^T, U) = -(U L_y^T, U L_y^T) = -\|U L_y^T\|_2^2$. The fourth term is

$$\beta ((|U| \odot |U|) \odot U, U) = h_x h_y \beta \left(\sum_{j=1}^{N_x} \sum_{k=1}^{N_y} |U_{j,k}|^4 \right) = \beta \|U\|_4^4.$$

Now the equation (2.22) can be rewritten as

$$i \left(\frac{dU}{dt}, U \right) - \|L_x U\|_2^2 - \|U L_y^T\|_2^2 + \beta \|U\|_4^4 = 0. \tag{2.23}$$

Taking the complex conjugate for every term in the equation (2.23), we get

$$-i \left(U, \frac{dU}{dt} \right) - \|L_x U\|_2^2 - \|U L_y^T\|_2^2 + \beta \|U\|_4^4 = 0. \tag{2.24}$$

Taking the difference between (2.23) and (2.24), we obtain $\frac{d}{dt} \|U\|_2^2 \equiv 0$. This completes the proof. \square

Theorem 2.4. *With the homogeneous Dirichlet boundary conditions, the scheme preserves the energy conservation law:*

$$\frac{d}{dt} E_h(t) \equiv 0. \tag{2.25}$$

Proof. Taking the inner product of the scheme (2.16) with $\frac{dU}{dt}$ yields

$$i \left(\frac{dU}{dt}, \frac{dU}{dt} \right) + \left(D_x U, \frac{dU}{dt} \right) + \left(U D_y^T, \frac{dU}{dt} \right) + \beta \left((|U| \odot |U|) \odot U, \frac{dU}{dt} \right) = 0.$$

Based on Lemma 2.2, we can obtain

$$i \left(\frac{dU}{dt}, \frac{dU}{dt} \right) - \left(L_x U, L_x \frac{dU}{dt} \right) - \left(U L_y^T, \frac{dU}{dt} L_y^T \right) + \beta \left((|U| \odot |U|) \odot U, \frac{dU}{dt} \right) = 0. \tag{2.26}$$

Next, take the complex conjugate for every term in (2.26), i.e.,

$$-i \left(\frac{dU}{dt}, \frac{dU}{dt} \right) - \left(L_x \frac{dU}{dt}, L_x U \right) - \left(\frac{dU}{dt} L_y^T, U L_y^T \right) + \beta \left((|U| \odot |U|) \odot \frac{dU}{dt}, U \right) = 0. \tag{2.27}$$

Taking the sum of the two equalities (2.26) and (2.27), we can derive

$$\frac{d}{dt} (-(L_x U, L_x U) - (U L_y^T, U L_y^T)) + \beta \left(|U| \odot |U|, \frac{d(|U| \odot |U|)}{dt} \right) \equiv 0.$$

From the above equation, we can get that

$$\frac{d}{dt} \left(-\|L_x U\|_2^2 - \|U L_y^T\|_2^2 + \frac{\beta}{2} \|U\|_4^4 \right) \equiv 0. \tag{2.28}$$

Now we have completed the proof for the energy conservation law (2.25). \square

3 Time integration

In the proceeding section, we have proved that the semi-discrete scheme (2.16) preserves mass and energy conservation. In order to extend the mass and energy conservation property to the fully discrete method, the usual choice of the time discretization scheme is the Crank-Nicolson method which can be proved to preserve the mass and energy conservation in fully-discrete formulation. Despite the property of preserving the conservation laws, solving such a nonlinear system is not practical due to extremely high time complexity. The linearized iteration algorithm [37] can be implemented to overcome the difficulty. However, the linearization procedure needs to reduce the time step to ensure the method convergent for the strong nonlinear problem. Therefore we implement the other time discretization method: the compact implicit integration factor (cIIF) method. The cIIF method is provided with the excellent stability condition (assuring unconditional linear stability with respect to both diffusion and nonlinear terms) and CPU efficiency which demands much less computational effort. The fully-discrete mass and energy conservation can be numerically observed for the cIIF method. Moreover, the numerical experiments in the next section show that the cIIF method is more efficient than the CN method. In the time discretization method, we set the time step as τ and define the time level as $t_n = n\tau$, $n = 0, 1, 2, \dots$

3.1 The Crank-Nicolson method

By applying the implicit midpoint method in time for (2.16), the Crank-Nicolson difference scheme in matrix formulation reads as follow:

$$i \frac{U^{n+1} - U^n}{\tau} + D_x U^{n+\frac{1}{2}} + U^{n+\frac{1}{2}} D_y^T + \beta \frac{|U^{n+1}|^2 + |U^n|^2}{2} U^{n+\frac{1}{2}} = 0, \quad (3.1)$$

where $U^{n+\frac{1}{2}} = \frac{U^{n+1} + U^n}{2}$. To check our method's capability of preserving the mass and energy conservation, we define the discretized mass and energy as

$$Q(n) = \|U^n\|^2, \quad E(n) = \|L_x U^n\|^2 + \|U^n L_y^T\|^2 - \frac{\beta}{4} \|U^n\|_4^4.$$

The conservation in the one-dimensional case has been proposed in [32]. We extend the mass and energy conservation for the two-dimensional fully discrete scheme.

Theorem 3.1. *The Crank-Nicolson scheme (3.1) preserves the mass conservation law in fully discrete formulation,*

$$Q(n+1) = Q(n) = \dots = Q(0). \quad (3.2)$$

Proof. These equalities are frequently used in the proof, listed as follows:

$$\operatorname{Re}(U^{n+\frac{1}{2}}, U^{n+1} - U^n) = \frac{\|U^{n+1}\|^2 - \|U^n\|^2}{2}, \quad (3.3)$$

$$\operatorname{Re}(D_x U^{n+\frac{1}{2}}, U^{n+1} - U^n) = \|L_x U^{n+1}\|^2 - \|L_x U^n\|^2, \quad (3.4)$$

$$\operatorname{Re}(U^{n+\frac{1}{2}} D_y^T, U^{n+1} - U^n) = \|U^{n+1} L_y^T\|^2 - \|U^n L_y^T\|^2, \quad (3.5)$$

which can be easily verified by the inner product definition (2.2) and Lemma 2.2 and we omit the proof.

Taking the inner product of the scheme (3.1) with $U^{n+\frac{1}{2}}$ yields

$$\begin{aligned} & \left(i \frac{U^{n+1} - U^n}{\tau}, U^{n+\frac{1}{2}} \right) + (D_x U^{n+\frac{1}{2}}, U^{n+\frac{1}{2}}) + (U^{n+\frac{1}{2}} D_y^T, U^{n+\frac{1}{2}}) \\ & + \beta \left(\frac{|U^{n+1}|^2 + |U^n|^2}{2} U^{n+\frac{1}{2}}, U^{n+\frac{1}{2}} \right) = 0. \end{aligned} \quad (3.6)$$

Based on Lemma 2.2, we can get

$$\left(i \frac{U^{n+1} - U^n}{\tau}, U^{n+\frac{1}{2}} \right) - \|L_x U^{n+\frac{1}{2}}\|^2 - \|U^{n+\frac{1}{2}} L_y^T\|^2 + \beta \left(\frac{|U^{n+1}|^2 + |U^n|^2}{2}, |U^{n+\frac{1}{2}}|^2 \right) = 0. \quad (3.7)$$

Taking the imaginary part, we can obtain

$$\|U^{n+1}\|^2 - \|U^n\|^2 = 0 \tag{3.8}$$

by using (3.3). We have completed the proof. \square

Theorem 3.2. *The Crank-Nicolson scheme (3.1) preserves the energy conservation law in fully discrete formulation,*

$$E(n + 1) = E(n) = \dots = E(0). \tag{3.9}$$

Proof. Taking the inner product of the scheme (3.1) with $U^{n+1} - U^n$ yields

$$\begin{aligned} & \left(i \frac{U^{n+1} - U^n}{\tau}, U^{n+1} - U^n \right) + (D_x U^{n+\frac{1}{2}}, U^{n+1} - U^n) + (U^{n+\frac{1}{2}} D_y^T, U^{n+1} - U^n) \\ & + \left(\beta \frac{|U^{n+1}|^2 + |U^n|^2}{2} U^{n+\frac{1}{2}}, U^{n+1} - U^n \right) = 0. \end{aligned} \tag{3.10}$$

With the equalities (3.4) and (3.5), we can get

$$i \frac{\|U^{n+1}\| - \|U^n\|^2}{\tau} - \|L_x U^{n+1}\|^2 + \|L_x U^n\|^2 - \|U^{n+1} L_y^T\|^2 + \|U^n L_y^T\|^2 + \frac{\beta}{4} (\|U^{n+1}\|_4^4 - \|U^n\|_4^4) = 0. \tag{3.11}$$

Taking the real part,

$$- \|L_x U^{n+1}\|^2 + \|L_x U^n\|^2 - \|U^{n+1} L_y^T\|^2 + \|U^n L_y^T\|^2 + \frac{\beta}{4} (\|U^{n+1}\|_4^4 - \|U^n\|_4^4) = 0. \tag{3.12}$$

This completes the proof. \square

3.2 The compact implicit integration factor method

The semi-discrete formulation (2.16) can be written into the following nonlinear complex ODE system:

$$\frac{dU}{dt} = AU + UB + F(U), \tag{3.13}$$

where $A = iD_x$, $B = iD_y^T$ and $F(U) = i\beta(|U| \odot |U|) \odot U$. The following derivation procedure is similar to the method in [26]. Multiplying (3.13) by the integration factor e^{-At} from the left and e^{-Bt} from the right, and integrating over one time step from t_n to t_{n+1} , we can obtain

$$U_{n+1} = e^{A\tau} U_n e^{B\tau} + e^{A\tau} \left(\int_0^\tau e^{-As} F(U(t_n + s)) e^{-Bs} ds \right) e^{B\tau}. \tag{3.14}$$

Then we approximate the integrand in (3.14) by using an $(r - 1)$ -th order Lagrange interpolation polynomial with interpolation points at $t_{n+1}, t_n, \dots, t_{n-r+2}$ to obtain the r -th order cIIF scheme

$$U_{n+1} = e^{A\tau} U_n e^{B\tau} + \tau \left(\alpha_1 F(U_{n+1}) + \sum_{j=0}^{r-2} \alpha_{-j} e^{(j+1)A\tau} F(U_{n-j}) e^{(j+1)B\tau} \right). \tag{3.15}$$

See [26] for the values of coefficients α_j , $j = 1, 0, \dots, 2 - r$. In this paper, the second-order (cIIF2) as well as the third-order (cIIF3) cIIF schemes are considered in an attempt to balance the spatial and temporal accuracy of the overall approach:

$$U_{n+1} = e^{A\tau} \left(U_n + \frac{\tau}{2} F(U_n) \right) e^{B\tau} + \frac{\tau}{2} F(U_{n+1}), \tag{3.16}$$

$$U_{n+1} = e^{A\tau} \left(U_n + \frac{2\tau}{3} F(U_n) \right) e^{B\tau} + \frac{5\tau}{12} F(U_{n+1}) - \frac{\tau}{12} e^{2A\tau} F(U_{n-1}) e^{2B\tau}. \tag{3.17}$$

However, the third-order cIIF3 scheme (3.17) is not selfstarting, in the sense that the first time step solution U_1 has to be provided by the other two-level scheme with a smaller time step. In our numerical simulation we use the cIIF2 scheme (3.16) with a time step $\frac{\tau}{10}$ to calculate the value $U(\cdot, \frac{\tau}{10})$, and then we use repeatedly the scheme (3.16) with timestep $\frac{\tau}{10}$ until we get the values U_1 . Then we go ahead to simulate the problem using the scheme (3.17) with time step τ .

Note that the four matrices $e^{A\tau}$, $e^{B\tau}$, $e^{2A\tau}$ and $e^{2B\tau}$ in (3.16)–(3.17) are $N_x \times N_x$ and $N_y \times N_y$, respectively. They have sizes of a one-dimensional problem. We only need to compute matrix exponentials for matrices with sizes of one-dimensional problems. Otherwise, the size of the non-compact implicit integration factor scheme is bigger than these orders of magnitude, which is $N_x N_y \times N_x N_y$. The compact implicit integration factor method not only saves storage critical for simulations with larger numbers of spatial grid points, but also needs much fewer operations.

3.3 The relation between the CN and cIIF methods

We have proposed two time integration methods: the CN and cIIF methods. In the following, we will analyze the two schemes to find the relation between them. The CN and cIIF2 methods both have the second-order time accuracy. Although a complete proof of the conservation cannot be presented for the cIIF2 method in this paper, we can show that the cIIF2 scheme (3.16) approximates the CN scheme (3.1) with the error $O(\tau^2)$.

Theorem 3.3. *The fully discrete formulation cIIF2 scheme (3.16) approximates the CN scheme (3.1) with the error $O(\tau^2)$.*

Proof. By the (1, 1) Padé approximation [25], the exponential matrices $e^{A\tau}$ and $e^{B\tau}$ can be computed as

$$e^{A\tau} = \left(I - \frac{A\tau}{2}\right)^{-1} \left(I + \frac{A\tau}{2}\right) + O(\tau^2), \quad e^{B\tau} = \left(I + \frac{B\tau}{2}\right) \left(I - \frac{B\tau}{2}\right)^{-1} + O(\tau^2), \quad (3.18)$$

where I represents the unit matrix. Substituting (3.18) into the second-order cIIF scheme (3.16), we have

$$U_{n+1} = \left(I - \frac{A\tau}{2}\right)^{-1} \left(I + \frac{A\tau}{2}\right) \left(U_n + \frac{\tau}{2} F(U_n)\right) \left(I + \frac{B\tau}{2}\right) \left(I - \frac{B\tau}{2}\right)^{-1} + \frac{\tau}{2} F(U_{n+1}) + O(\tau^2). \quad (3.19)$$

Multiplying $\left(I - \frac{A\tau}{2}\right)$ on the left and $\left(I - \frac{B\tau}{2}\right)$ on the right for (3.19) yields

$$\begin{aligned} &\left(I - \frac{A\tau}{2}\right) U_{n+1} \left(I - \frac{B\tau}{2}\right) \\ &= \left(I + \frac{A\tau}{2}\right) \left(U_n + \frac{\tau}{2} F(U_n)\right) \left(I + \frac{B\tau}{2}\right) + \left(I - \frac{A\tau}{2}\right) \frac{\tau}{2} F(U_{n+1}) \left(I - \frac{B\tau}{2}\right) + O(\tau^2). \end{aligned} \quad (3.20)$$

Further expanding (3.20) and putting the term including τ^2 into $O(\tau^2)$, we get

$$U_{n+1} - \frac{A\tau}{2} U_{n+1} - U_{n+1} \frac{B\tau}{2} = U_n + \frac{A\tau}{2} U_n + U_n \frac{B\tau}{2} + \frac{\tau}{2} (F(U_n) + F(U_{n+1})) + O(\tau^2). \quad (3.21)$$

Remembering $A = iD_x$, $B = iD_y^T$ and $F(U) = i\beta(|U| \odot |U|) \odot U$, we can get the following after some simple calculation:

$$\begin{aligned} &i \frac{U^{n+1} - U^n}{\tau} + D_x U^{n+\frac{1}{2}} + U^{n+\frac{1}{2}} D_y^T + \beta \frac{|U^{n+1}|^2 + |U^n|^2}{2} U^{n+\frac{1}{2}} \\ &= \frac{\beta}{4} (|U^{n+1}|^2 - |U^n|^2) (U^{n+1} - U^n) + O(\tau^2). \end{aligned} \quad (3.22)$$

Based on the Taylor expansion, the term $(|U^{n+1}|^2 - |U^n|^2)(U^{n+1} - U^n)$ for the solution can be considered as $O(\tau^2)$. We finish the proof. \square

4 Numerical experiments

In this section, we present some numerical experiments to test the performance of the proposed WSGD-clIF schemes (3.16) and (3.17). In all the numerical experiments, we use a uniform spatial step size along each direction, i.e., that $h_x = h_y = h$. The theoretical analysis shows that the solution $u(x, y, t)$ of two-dimensional FNLS equation (1.1) blows up in finite time if the initial energy $E(0) < 0$ [3]. We will verify this conclusion by some numerical examples. Firstly, we set the initial condition with positive energy and find no blow-up phenomenon. Then we take a unique point as the origin of the radially symmetric initial value to find the L^2 -concentration phenomenon. All the computations are performed in Matlab platform based on a ThinkPad desktop with i3-3110 CPU and 4 GB memory.

Example 4.1. In this example, we perform the computation on a square domain $[-10, 10]^2$ with $\beta = 1$. The initial data are given as $u(x, y, 0) = \frac{2}{\sqrt{\pi}} \exp(-(x^2 + y^2))$. We first validate the discrete conservation laws. Here, we choose $h = 0.05$ and $\tau = 0.01$. Table 1 presents the values of the mass $Q(n)$ and

Table 1 The values of $Q(n)$ and $E(n)$ at different time with $\tau = h = 0.05$ and $h = 0.01$

T	$\alpha = 1.3$		$\alpha = 1.5$		$\alpha = 1.8$	
	$Q(n)$	$E(n)$	$Q(n)$	$E(n)$	$Q(n)$	$E(n)$
$T = 0$	2.0000169	2.6644232	2.0000092	2.8003142	2.0000269	3.0969083
$T = 2$	2.0000269	2.6644239	2.0000269	2.8003146	2.0000270	3.0969082
$T = 4$	2.0000270	2.6644237	2.0000270	2.8003144	2.0000270	3.0969081
$T = 6$	2.0000270	2.6644237	2.0000270	2.8003144	2.0000270	3.0969083
$T = 8$	2.0000268	2.6644231	2.0000269	2.8003143	2.0000270	3.0969080
$T = 10$	2.0000269	2.6644236	2.0000270	2.8003143	2.0000270	3.0969088

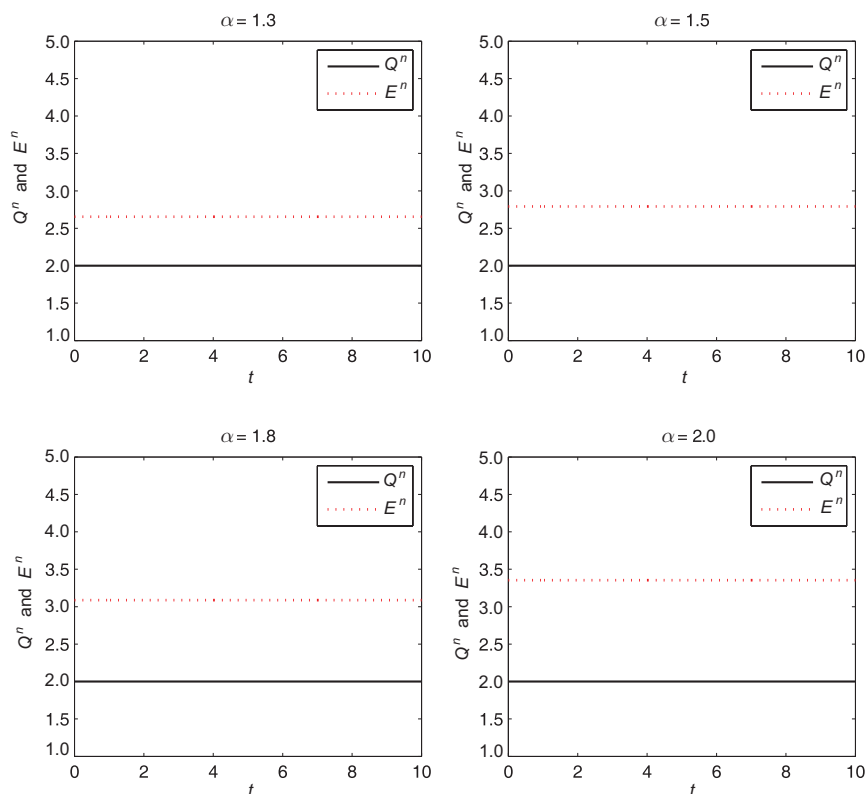


Figure 1 Evolution of mass Q^n and energy E^n for different values of α

Table 2 The space errors and convergence orders for the second-order WSGD method in Example 4.1

m	$\alpha = 1.3$		$\alpha = 1.5$		$\alpha = 1.8$	
	Error	Order	Error	Order	Error	Order
5	6.02E-2	–	7.16E-2	–	8.56E-2	–
6	1.97E-2	1.61	2.35E-2	1.61	2.69E-2	1.67
7	5.30E-3	1.90	6.31E-3	1.90	6.85E-3	1.97
8	1.11E-3	2.25	1.32E-3	2.26	1.39E-3	2.29

Table 3 The temporal errors and convergence orders for the cIIF2 scheme in Example 4.1

τ	$\alpha = 1.3$		$\alpha = 1.5$		$\alpha = 1.8$	
	Error	Order	Error	Order	Error	Order
$2d - 2$	2.04E-3	–	2.51E-4	–	6.80E-5	–
$1d - 2$	5.16E-4	1.98	6.31E-5	2.00	1.70E-5	2.00
$5d - 3$	1.29E-4	2.00	1.58E-5	2.00	4.26E-6	1.99
$2.5d - 3$	3.24E-5	1.99	3.95E-6	2.00	1.06E-6	2.01

Table 4 The space errors and convergence orders for the third-order WSGD method in Example 4.1

m	$\alpha = 1.3$		$\alpha = 1.5$		$\alpha = 1.8$	
	Error	Order	Error	Order	Error	Order
5	1.20E-1	–	1.03E-1	–	9.81E-2	–
6	2.41E-2	2.32	2.07E-2	2.32	1.83E-2	2.42
7	3.55E-3	2.76	2.91E-3	2.83	2.05E-3	3.16
8	4.03E-4	3.14	3.12E-4	3.22	1.82E-4	3.50

Table 5 The temporal errors and convergence orders for the cIIF3 scheme in Example 4.1

τ	$\alpha = 1.3$		$\alpha = 1.5$		$\alpha = 1.8$	
	Error	Order	Error	Order	Error	Order
$2d - 2$	9.06E-5	–	2.22E-5	–	1.08E-5	–
$1d - 2$	1.26E-5	2.84	2.96E-6	2.91	1.44E-6	2.91
$5d - 3$	1.65E-6	2.93	3.81E-7	2.96	1.85E-7	2.96
$2.5d - 3$	2.11E-7	2.97	4.84E-8	2.98	2.35E-8	2.98

Table 6 The CPU time (s) for CN and cIIF schemes

h	$\alpha = 1.3$		$\alpha = 1.5$		$\alpha = 1.8$	
	CN	cIIF2	CN	cIIF2	CN	cIIF2
0.8	24.94	1.335E-7	25.87	0.475	27.79	0.446
0.4	463.50	1.528	445.60	1.449	461.80	1.333
0.2	–	5.675	–	5.437	–	5.279

energy $E(n)$ at different time for $\alpha = 1.3$, $\alpha = 1.5$ and $\alpha = 1.8$, respectively. Figure 1 depicts the evolution of the discrete mass and energy in time interval $[0, 10]$. We can observe that the WSGD-cIIF scheme conserves the mass and energy exactly from Figure 1 and Table 1. Nevertheless, unlike the mass conservation which is independent of the value of α , the energy increases as α grows.

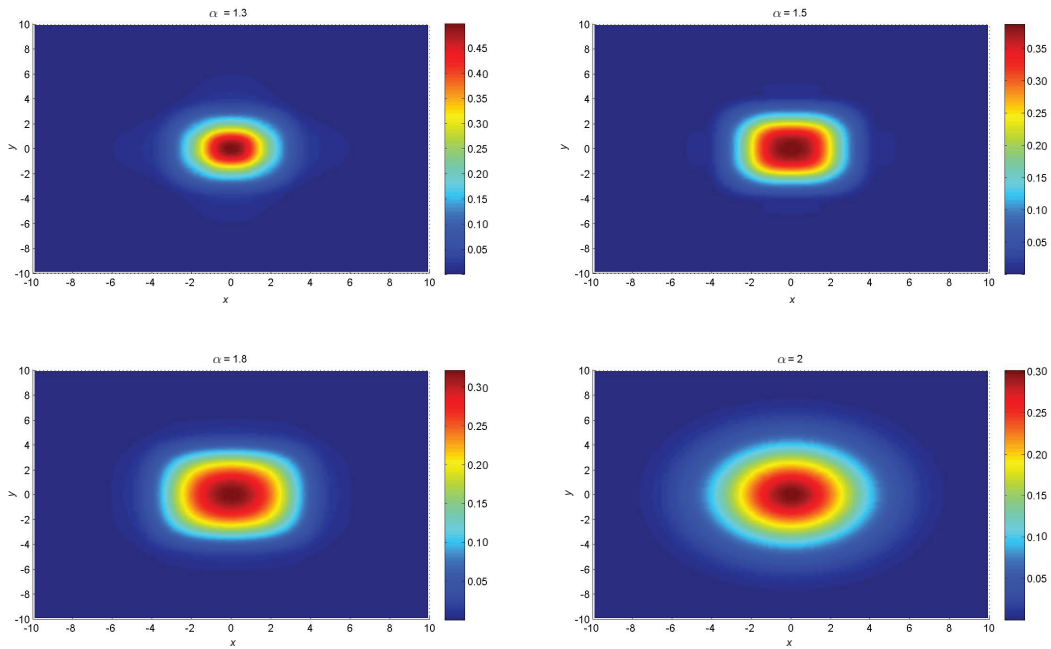


Figure 2 Profile plot of $|u|$ for different values of α at time $t = 1$ in Example 4.1

Table 7 The CPU time and $|U|_{\max}$ for CN and cIIF2 schemes in Example 4.2

	$\alpha = 1.3$		$\alpha = 1.5$		$\alpha = 1.8$	
	$ U _{\max}$	CPU (s)	$ U _{\max}$	CPU (s)	$ U _{\max}$	CPU (s)
CN	14.55	1329.70	16.48	984.44	20.18	756.12
cIIF2	30.64	347.74	38.36	269.49	53.99	188.07

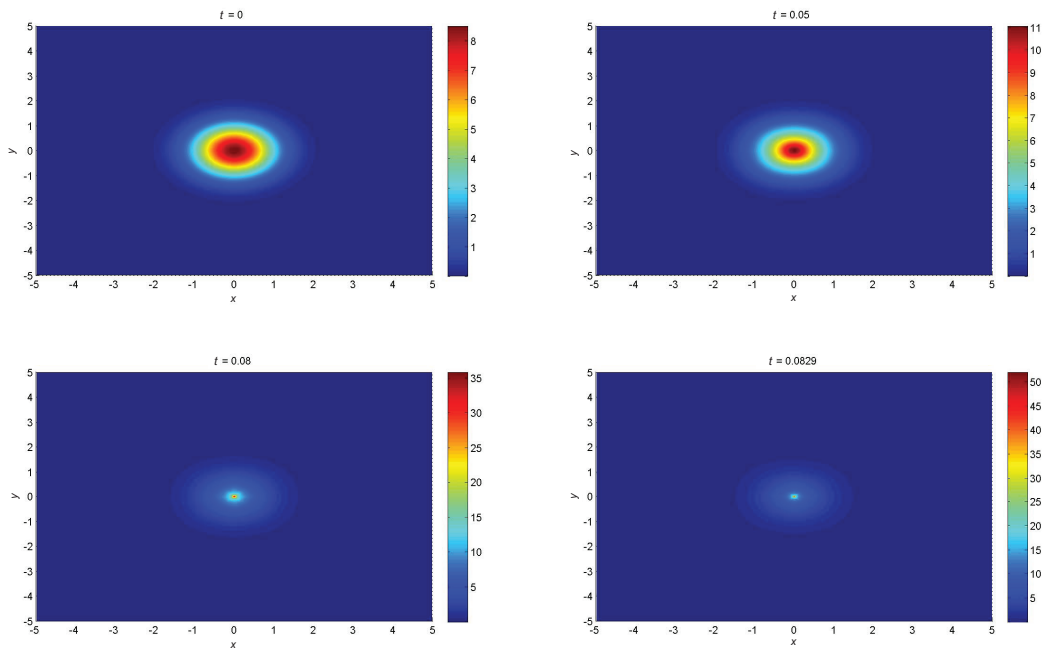


Figure 3 Images $|u|$ for the numerical solution of the FNLS equation in Example 4.2 with $\alpha = 1.3$ at different time

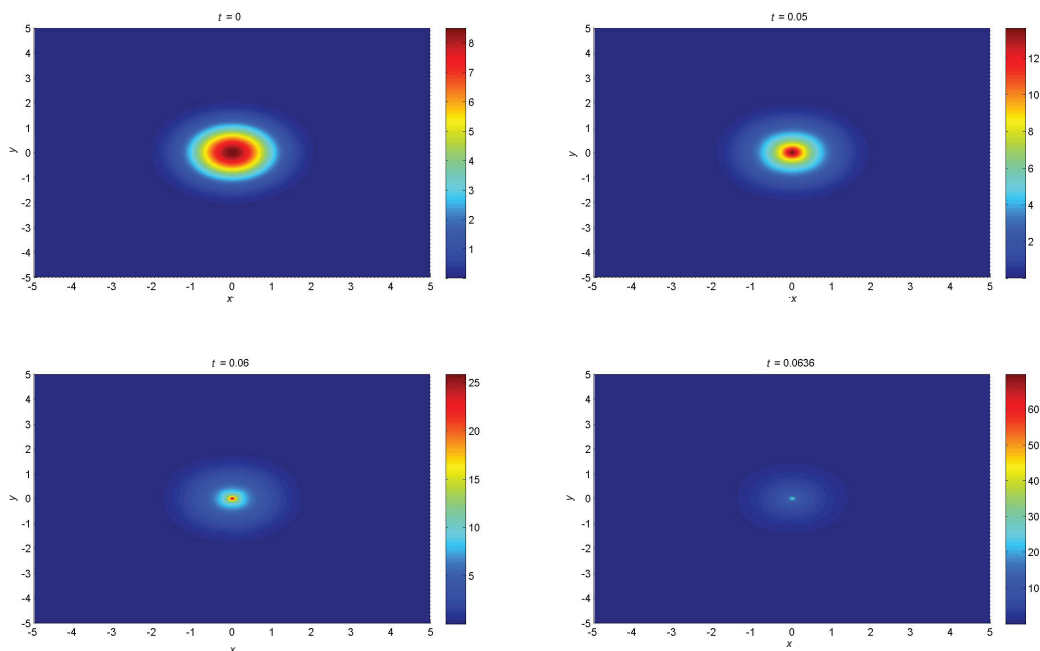


Figure 4 Images $|u|$ for the numerical solution of the FNLSE equation in Example 4.2 with $\alpha = 1.5$ at different time

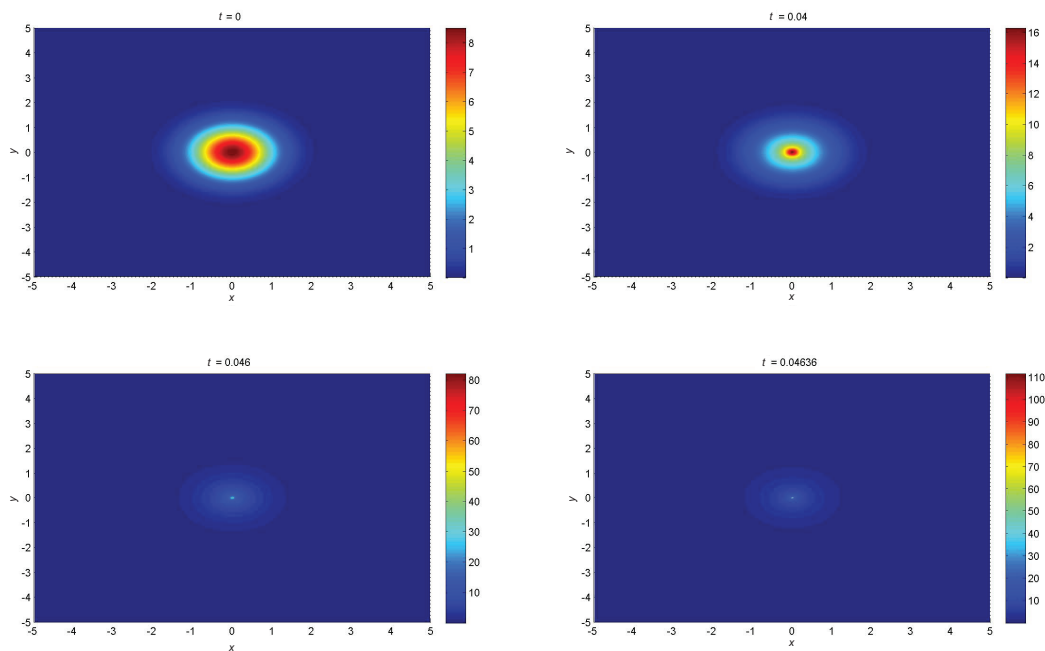


Figure 5 Images $|u|$ for the numerical solution of the FNLSE equation in Example 4.2 with $\alpha = 1.8$ at different time

We use two numerical schemes: the second-order WSGD method with the cIIF2 scheme and the third-order WSGD method with the cIIF3 scheme to demonstrate the accuracy of the space and time discretization. Denote by $\{U(\tau, h)\}$ the numerical solution of the space grid h and the time grid τ at time T . The error in the spatial direction with sufficiently small time step τ is calculated by

$$e(h) = \|U(\tau, h) - U(\tau, h/2)\|_{\infty}$$

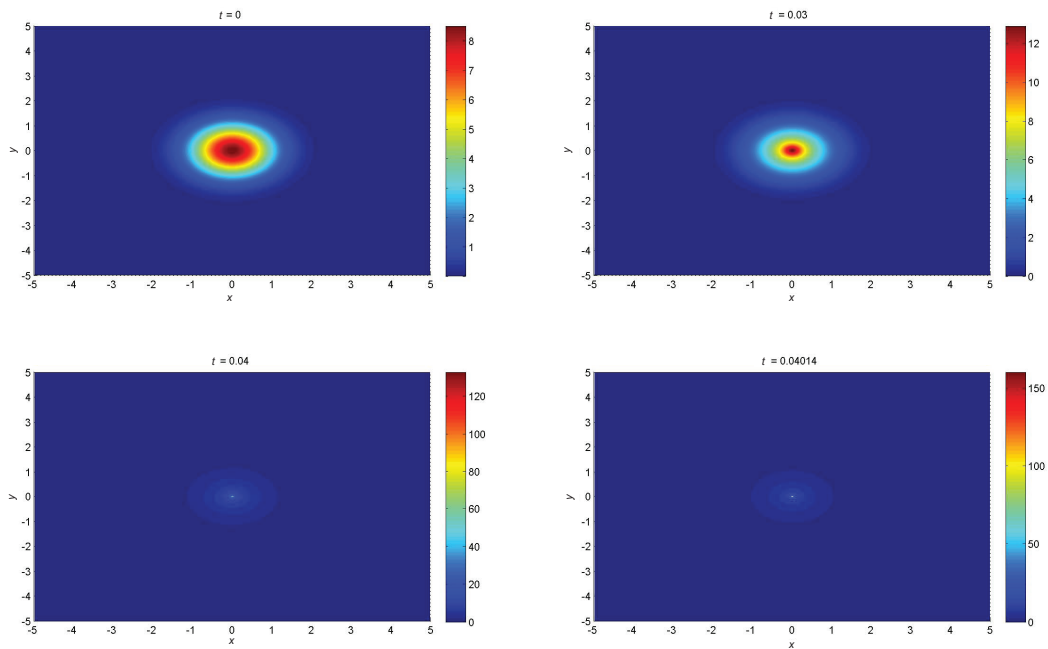


Figure 6 Images $|u|$ for the numerical solution of the FNLSE equation in Example 4.2 with $\alpha = 2$ at different time

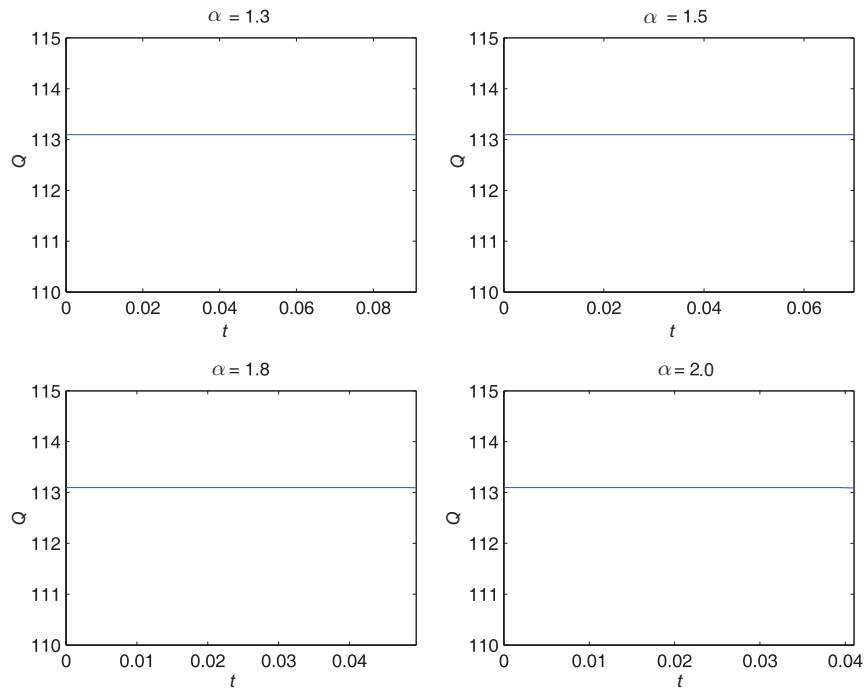


Figure 7 Evolution of mass Q^n for different values of α

and the error in the temporal direction with sufficiently small h is similarly calculated by

$$e(\tau) = \|U(\tau, h) - U(\tau/2, h)\|_\infty.$$

The orders of convergence in space and time are computed as

$$q = \log_2(e(h)/e(h/2)) \quad \text{and} \quad p = \log_2(e(\tau)/e(\tau/2)),$$

respectively. Table 2 displays the space errors of the second-order WSGD scheme with different

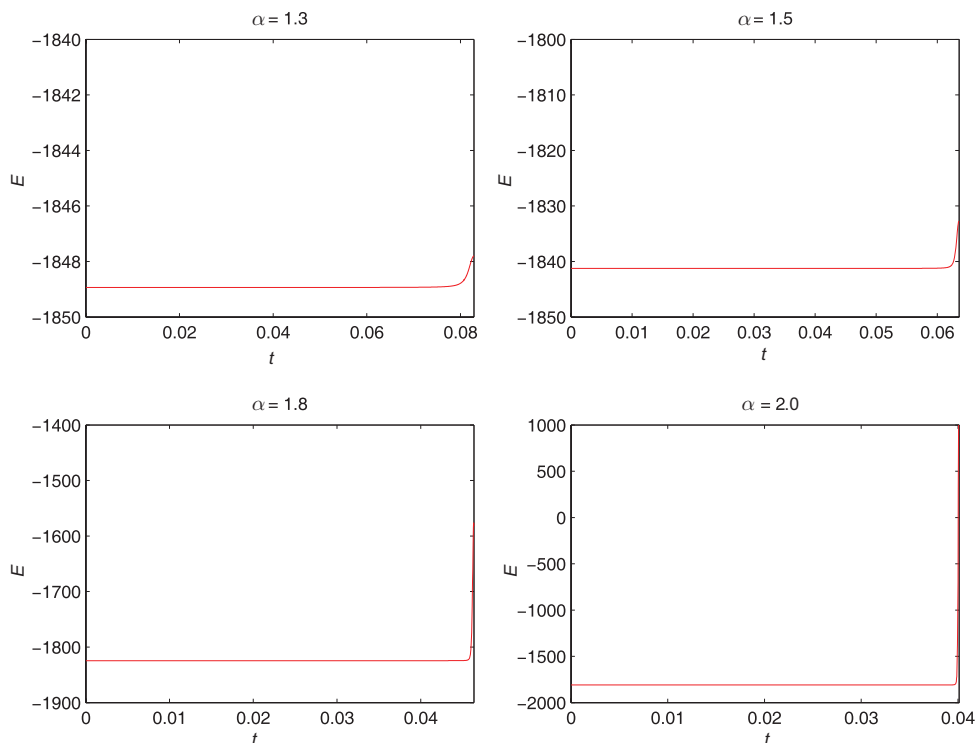


Figure 8 Evolution of energy E^n for different values of α

space grids $h = \frac{20}{2^m}$ and values of α . The order of convergence is computed using a very small time step $\tau = 1d - 3$. In Table 3, the temporal errors and convergence orders of the cIIF2 scheme are given for different time steps and α when the space grid is fixed to be $h = 0.1$. From Tables 2 and 3, we conclude that the convergence rate in space and time is second-order. The space and temporal errors of the third-order WSGD method coupled with cIIF3 schemes are shown in Tables 4 and 5. We can observe that we obtain desired accuracy orders for all cases.

Next, we show the efficiency of our proposed WSGD-cIIF2 scheme by comparing the CPU time with the WSGD-CN scheme. Choosing $\tau = 0.01$ the CPU time is obtained at the final time $T = 10$ with different h . As seen in Table 6, the CN scheme on our desktop with 4 GB RAM runs out of memory when $N_x = N_y = 100$ because of storing matrices with a size of $10^4 \times 10^4$. On the other hand, the cIIF2 scheme can run on the same machine with much larger N_x because of its small memory requirement. For smaller N_x such as $N_x = 50$, although the machine has enough memory for the CN scheme, it needs almost 300 times more CPU time to achieve the same accuracy as cIIF2. Therefore we can draw that the cIIF2 scheme is more efficient than the CN scheme, especially for the long time simulation of the large size problem.

Finally, we use the WSGD scheme (2.16) coupled with the cIIF scheme (3.16) to simulate the dynamics of the solution. The mesh steps used are $\tau = 0.01$ and $h = 0.1$. We can compute the discretized energy of the initial condition by (2.20) to obtain that $E(0) = 2.66$, $E(0) = 2.79$, $E(0) = 3.09$ and $E(0) = 3.35$ for $\alpha = 1.3$, $\alpha = 1.5$, $\alpha = 1.8$ and $\alpha = 2$, respectively. There is no blow-up because of the positive initial energy. This agrees with the theoretical results. The contours of the modulus of the numerical function at $t = 1$ are shown in Figure 2 with different α . Especially, comparing the solutions for $\alpha = 1.3$, $\alpha = 1.5$ and $\alpha = 1.8$ with the classical case ($\alpha = 2$) for reference, we can observe that the wave function decays significantly faster and the wave shape becomes taller and steeper for progressively decreasing α . These phenomena display that, the smaller the fractional order α is, the stronger the nonlocal effect is.

Example 4.2. In this example we show singular solutions for the FNLS equation (1.1) with the same condition except the initial condition that is chosen as $u(x, y, 0) = 6\sqrt{2}e^{-(x^2+y^2)}$. The initial energy for $\alpha = 1.3$, $\alpha = 1.5$, $\alpha = 1.8$ and $\alpha = 2$ is computed as $E(0) = -1848.9$, $E(0) = -1841.2$, $E(0) = -1824.5$

and $E(0) = -1809.6$, respectively. The negative initial energy means that the solution will blow up in finite time. We give the CPU time comparison of the CN and cIIF2 schemes for the blow-up case. By choosing $h = 0.2$ for the CN scheme and $h = 0.05$ for the cIIF2 scheme, the CPU time and the maximum absolute value of the solution, $|U|_{\max}$, are obtained at the blow-up time. We list the CPU time and $|U|_{\max}$ with α in Table 7. As seen in Table 7, the CN scheme needs more CPU time than the cIIF2 scheme even with smaller grid numbers. The height of blow-up solutions it can reach is lower, which means that the CN scheme is not appropriate to simulate the blow-up solution in two dimensions. By contrast the cIIF2 scheme is a good choice for two-dimensional fractional NLS equations. Figures 3–6 show the modulus of the solution approximated using the WSGD-cIIF2 scheme with $N_x = N_y = 512$ and $\tau = 2d - 5$. The blow-up effect is obtained in finite time with different α . These plots show that the blow-up time gets smaller and the tall peak gets sharper for progressively increasing α .

We also show the evolution of mass and energy for the blow-up solution in Figures 7 and 8 for Example 4.2. Figure 7 shows that the mass could keep conservation till the solution blows up. However, as shown in Figure 8, the energy conservation is violated because the energy contains the gradient term which increases rapidly with blow-up solutions.

5 Conclusion

In this paper we have combined the WSGD space discretization method with the cIIF time discretization method for computing the two-dimensional FNLS equation. We have proved that the WSGD method can keep the conservation law in mass and energy in semi-discrete and fully-discrete formulation with the Crank-Nicolson time scheme. Moreover, this method has uniform second- and third-order accuracy in space and time. The numerical examples confirmed the excellent qualities of our method. In future work, this method will be extended to the FNLS equation with damping terms or an angular momentum rotation term as well as coupled FNLS equations.

Acknowledgements This work was supported by National Natural Science Foundation of China (Grant Nos. 61573008 and 61703290), Laboratory of Computational Physics (Grant No. 6142A0502020717) and National Science Foundation of USA (Grant No. DMS-1620108).

References

- 1 Aboelenen T. A high-order nodal discontinuous Galerkin method for nonlinear fractional Schrödinger type equations. *Commun Nonlinear Sci Numer Simul*, 2018, 54: 428–452
- 2 Bhrawy A H, Abdelkawy M A. A fully spectral collocation approximation for multi-dimensional fractional Schrödinger equations. *J Comput Phys*, 2015, 294: 462–483
- 3 Boulenger T, Himmelsbach D, Lenzmann E. Blowup for fractional NLS. *J Funct Anal*, 2016, 271: 2569–2603
- 4 Çelik C, Duman M. Crank-Nicolson method for the fractional diffusion equation with the Riesz fractional derivative. *J Comput Phys*, 2012, 231: 1743–1750
- 5 Chang Q, Jia E, Sun W. Difference schemes for solving the generalized nonlinear Schrödinger equation. *J Comput Phys*, 1999, 148: 397–415
- 6 Dehghan M, Taleei A. A compact split-step finite difference method for solving the nonlinear Schrödinger equations with constant and variable coefficients. *Comput Phys Comm*, 2010, 181: 43–51
- 7 Duan B, Zheng Z, Cao W. Finite element method for a kind of two-dimensional space-fractional diffusion equation with its implementation. *Amer J Comput Math*, 2015, 5: 135
- 8 Duo S, Zhang Y. Mass-conservative Fourier spectral methods for solving the fractional nonlinear Schrödinger equation. *Comput Math Appl*, 2016, 71: 2257–2271
- 9 Fröhlich J, Jonsson B L G, Lenzmann E. Boson stars as solitary waves. *Comm Math Phys*, 2007, 274: 1–30
- 10 Gong Y, Wang Q, Wang Y, et al. A conservative Fourier pseudo-spectral method for the nonlinear Schrödinger equation. *J Comput Phys*, 2017, 328: 354–370
- 11 Hou T, Tang T, Yang J. Numerical analysis of fully discretized Crank-Nicolson scheme for fractional-in-space Allen-Cahn equations. *J Sci Comput*, 2017, 72: 1214–1231
- 12 Ionescu A D, Pusateri F. Nonlinear fractional Schrödinger equations in one dimension. *J Funct Anal*, 2014, 266: 139–176

- 13 Ji C C, Sun Z Z. A high-order compact finite difference scheme for the fractional sub-diffusion equation. *J Sci Comput*, 2015, 64: 959–985
- 14 Khaliq A Q M, Liang X, Furati K M. A fourth-order implicit-explicit scheme for the space fractional nonlinear Schrödinger equations. *Numer Algorithms*, 2017, 75: 147–172
- 15 Kirkpatrick K, Lenzmann E, Staffilani G. On the continuum limit for discrete NLS with long-range lattice interactions. *Comm Math Phys*, 2013, 317: 563–591
- 16 Klein C, Sparber C, Markowich P. Numerical study of fractional nonlinear Schrödinger equations. *Proc Math Phys Eng Sci*, 2014, 470: 20140364
- 17 Laskin N. Fractional quantum mechanics. *Phys Rev E*, 2000, 62: 3135–3145
- 18 Laskin N. Fractional Schrödinger equation. *Phys Rev E*, 2002, 66: 056108
- 19 Lenzmann E. Well-posedness for semi-relativistic Hartree equations of critical type. *Math Phys Anal Geom*, 2007, 10: 43–64
- 20 Li M, Huang C, Wang P. Galerkin finite element method for nonlinear fractional Schrödinger equations. *Numer Algorithms*, 2017, 74: 499–525
- 21 Liang X, Khaliq A Q M, Bhatt H, et al. The locally extrapolated exponential splitting scheme for multi-dimensional nonlinear space-fractional Schrödinger equations. *Numer Algorithms*, 2017, 76: 939–958
- 22 Magin R L, Abdullah O, Baleanu D, et al. Anomalous diffusion expressed through fractional order differential operators in the Bloch-Torrey equation. *J Magnet Reson*, 2008, 190: 255–270
- 23 Meerschaert M M, Tadjeran C. Finite difference approximations for fractional advection-dispersion flow equations. *J Comput Appl Math*, 2004, 172: 65–77
- 24 Merle F, Tsutsumi Y. L^2 concentration of blow-up solutions for the nonlinear Schrödinger equation with critical power nonlinearity. *J Differential Equations*, 1990, 84: 205–214
- 25 Moler C, Loan C V. Nineteen dubious ways to compute the exponential of a matrix, twenty-five years later. *SIAM Rev*, 2003 45: 3–49
- 26 Nie Q, Wan F Y M, Zhang Y, et al. Compact integration factor methods in high spatial dimensions. *J Comput Phys*, 2008, 227: 5238–5255
- 27 Nie Q, Zhang Y, Zhao R. Efficient semi-implicit schemes for stiff systems. *J Comput Phys*, 2006, 214: 521–537
- 28 Obrecht C. Remarks on the full dispersion Davey-Stewartson systems. *Commun Pure Appl Anal*, 2015, 14: 1547–1561
- 29 Ortigueira M D. Riesz potential operators and inverses via fractional centred derivatives. *Int J Math Math Sci*, 2006, 2006: 1–12
- 30 Tian W, Zhou H, Deng W. A class of second order difference approximations for solving space fractional diffusion equations. *Math Comput*, 2015, 84: 1703–1727
- 31 Wang D, Zhang L, Nie Q. Array-representation integration factor method for high-dimensional systems. *J Comput Phys*, 2014, 258: 585–600
- 32 Wang P, Huang C. An energy conservative difference scheme for the nonlinear fractional Schrödinger equations. *J Comput Phys*, 2015, 293: 238–251
- 33 Wang P, Huang C. Split-step alternating direction implicit difference scheme for the fractional Schrödinger equation in two dimensions. *Comput Math Appl*, 2016, 71: 1114–1128
- 34 Xu Y, Shu C. Local discontinuous Galerkin methods for nonlinear Schrödinger equations. *J Comput Phys*, 2005, 205: 72–97
- 35 Yang Q, Liu F, Turner I. Numerical methods for fractional partial differential equations with Riesz space fractional derivatives. *Appl Math Model*, 2010, 34: 200–218
- 36 Yang Q, Turner I, Liu F, et al. Novel numerical methods for solving the time-space fractional diffusion equation in two dimensions. *SIAM J Sci Comput*, 2011, 33: 1159–1180
- 37 Yang Z. A class of linearized energy-conserved finite difference schemes for nonlinear space-fractional Schrödinger equations. *Int J Comput Math*, 2016, 93: 609–626
- 38 Zhang R, Yu X, Li M, et al. A conservative local discontinuous Galerkin method for the solution of nonlinear Schrödinger equation in two dimensions. *Sci China Math*, 2017, 60: 2515–2530
- 39 Zhang R, Zhu J, Yu X, et al. A conservative spectral collocation method for the nonlinear Schrödinger equation in two dimensions. *Appl Math Comput*, 2017, 310: 194–203
- 40 Zhao X, Sun Z, Hao Z. A fourth-order compact ADI scheme for two-dimensional nonlinear space fractional Schrödinger equation. *SIAM J Sci Comput*, 2014, 36: 2865–2886